© Artificial Intelligence in Vision and Ophthalmology 2026; 2:1-10
Original article
https://doi.org/10.35119/aivo.v2i1.161

Analysis of the anatomical and functional ocular changes related to spaceflight

Gal Antman[1,2,3], Irit Bahar[1,2], Alon Tiosano[1,2], Alon Harris[3], Yamit Cohen-Tayar[1,2], Yair Zimmer[4], Amoy Fraser[5], Mehul Patel[5], Iftach Yassur[1,2], Itay Gabbay[1,2], Yehonatan Weinberger[1,2], Keren Wood[3], Orly Gal-Or[1,2]

[1]Department of Ophthalmology, Rabin Medical Center, Petach Tikva, Israel; [2]Faculty of Medicine, Tel Aviv University, Tel Aviv, Israel; [3]Department of Ophthalmology, Icahn School of Medicine at Mount Sinai, New York, NY, USA; [4]School of Medical Engineering, Afeka Tel Aviv College of Engineering, Tel Aviv, Israel; [5]Deparment of Ophthalmology, University of Central Florida, Orlando, FL, USA

Abstract

Purpose: To describe novel early changes in ocular physiology following short-duration exposure to microgravity.
Observations: The subject was a 64-year-old astronaut who participated in the AX-1 mission that was sent to the International Space Station by AXIOM Space and the National Aeronautics and Space Administration (NASA) in April 2022 for 17 days. Comprehensive multimodal preflight and postflight ophthalmic examinations were performed, including anterior and posterior segment imaging and head magnetic resonance imaging (MRI). In addition, optical coherence tomography angiography (OCTA), which is not part of the standard NASA protocol, was conducted for the first time in this setting in the medical literature. Automated image processing was used to quantify flow signal pixels from the retina or choroid for separate analysis. The subject reported a new-onset need for reading glasses while in space. Mild widening of the optic nerve sheaths was found on MRI. OCTA studies demonstrated a significant postflight decrease in macular choroidal flow signals by 29% in the right eye and 11% in the left eye, and in retinal flow signals by 8.5% and 6.5%, respectively ($p < 0.0001$ for both factors for both eyes). Focal alterations were noted in choroidal thickness and Haller's vessel diameter, which did not reach statistical significance.

Correspondence: Gal Antman, MD, Department of Ophthalmology, Rabin Medical Center – Beilinson Hospital, 39 Jabotinski St., Petach Tikva 4941492, Israel.
E-mail: antmangal@gmail.com

Conclusion: A significant decrease in macular choroidal and retinal blood flow was observed in an astronaut after a short-duration spaceflight. These changes may serve as possible biomarkers of spaceflight-associated neuro-ocular syndrome and warrant further investigation. We recommend that future spaceflight evaluations include OCTA in the standard protocol.

Keywords: eye physiology, optical coherence tomography angiography, spaceflight, spaceflight-associated neuro-ocular syndrome

Introduction

Ocular changes following exposure to gravitational alterations have been recognized since the beginning of the spaceflight era.[1] They can occur after both short- and long-duration flights, along with other systemic and neurological changes.[1] Physiologically, early hyperopic refractive shifts have been reported, starting in-flight and sometimes lasting for months after the return to Earth.[1] Changes that appear later have been more thoroughly described in the medical literature. In 2011, the term spaceflight-associated neuro-ocular syndrome (SANS) was introduced to describe the group of signs and symptoms reported in astronauts following long-duration space missions.[2] The most widely observed ocular structural findings were hyperopic shift, globe flattening, choroidal folds, optic disc edema, and cotton wool spots, some of which persisted for years.[3,4] Besides participation in long spaceflights, risk factors associated with SANS include lack of proper nutrition, high salt intake, and vitamin insufficiency.[1,4]

The underlying pathophysiological mechanism of SANS is still not fully understood. Most updated theories point to a cerebral-ocular fluid imbalance. Specifically, fluid shifts secondary to the microgravity environment lead to an increase in intracranial pressure (ICP), and the resulting disequilibrium with the gravity-related changes in intraocular pressure (IOP) affects the translaminar pressure gradient (TLPD).[5] While microgravity-associated increases in ICP are believed to reduce the TLPD, current evidence does not support a sustained inversion of this gradient.[3] A relative reduction in TLPD alone may be sufficient to impair axoplasmic flow and venous outflow at the optic nerve head without requiring reversal of pressure polarity. The fluid apparently enters from the optic nerve capillaries, peripapillary choroid, vitreous, and glymphatic system.[5] According to transcranial studies, cerebral autoregulation is impaired in long-duration, but not short-duration, spaceflight.[5]

Diagnostic procedures used to evaluate the eye in astronauts included ophthalmologic examinations, magnetic resonance imaging (MRI), optical coherence tomography (OCT), fundoscopy, orbital ultrasonography, and lumbar puncture.[1] All revealed alterations related to spaceflight. However, data from optical coherence

tomography angiography (OCTA) are so far unavailable in this setting. OCTA is a noninvasive motion-contrast imaging modality which allows for visualization of the retinal and choroidal vasculature by mapping erythrocyte movement in sequential OCT B-scans.[6] Along with enhanced depth imaging (EDI), it may serve as a promising tool for the comprehensive understanding of space-related ocular physiology and SANS.

The objective of this report was to apply OCTA to capture early changes in ocular morphology in an astronaut before and soon after 17 days of spaceflight and to assess these changes as possible biomarkers for SANS. A search of the literature in April 2026 utilizing PubMed and Google Scholar (keywords used as search terms: Space and Retina and Choroid and OCTA and SANS) did not yield any prior reports of OCTA and microgravity.

Methods

The AX-1 mission, the first private astronaut mission to the International Space Station, was launched by AXIOM Space and the National Aeronautics and Space Administration (NASA) in April 2022. Its four crew members were scheduled to spend 17 days in a microgravity environment. One of the crew was a 64-year-old male astronaut who was the subject of the present case report. He had no prior ocular disorders besides mild presbyopia (corresponding to age) and had never undergone any eye treatments. Data were collected from full clinical and imaging ophthalmic evaluation of the subject at the University of Central Florida, conducted several days before the flight (preflight session) and less than 24 hours after his return to Earth (postflight session). The study was conducted in accordance with the Declaration of Helsinki, and the study protocol was approved by the Institutional Review Boards of Rabin Medical Center, Petach Tikva, Israel and the University of Central Florida, Orlando, Florida, USA.

Clinical and imaging evaluation

The preflight and postflight clinical evaluations included uncorrected visual acuity (UCVA), best-corrected visual acuity (BCVA), color vision (Ishihara plates), axial protrusion of the globe (Hertel exophthalmometer), pupillary reaction, IOP (Tonopen, Reichert Inc, NY, USA) (average of three measurements), tear breakup time, pachymetry, slit-lamp examination, and dilated fundoscopy.

Visual field examination was performed using the standard Swedish interactive threshold algorithm (SITA) 24-2 protocol (Humphrey Field Analyzer, Carl Zeiss Meditec, Dublin, CA, USA), in addition to corneal tomography (Galilei Topographer, Ziemer Ophthalmic Systems, Port, Switzerland); ultrasonography (Quantal, Ophthalmic US Platform, Quantal Medical, Auvergne, France(; biometry (IOL Master 700, Zeiss Medical Technology, Obertkochen, Germany); and MRI, all part

of the Sheba Medical Center protocol.

Multicolor imaging and fundus autofluorescence scans were collected (Spectralis, Heidelberg Engineering, Heidelberg, Germany). A published NASA protocol was used for OCT imaging with EDI and anterior chamber imaging.[3] All OCT images were obtained with Spectralis OCT2 systems. Scans were centered on the macula and optic nerve head and included a 193-line EDI (20°) raster scan. Additionally, retinal nerve fiber layer thickness, Bruch's membrane opening area, and minimum rim width were measured.

OCTA imaging, which is not part of the NASA protocol and was used here for the first time in this setting, included a 10° field of view with 512 B-scans centered on the macula (Spectralis). The scans were performed preflight and repeated postflight by the same operator using the follow-up and automatic real-time tracking. Projection artifact removal was applied during data acquisition and analysis.

OCTA analysis

To calculate the preflight and postflight flow signals, data were exported, and a processing algorithm was applied to two sets of 512 JPEG structural OCT and OCTA flow data images displaying 512 retinal slices (Fig. 1). Image processing (Fig. 2A-C) involved separation to regions above and below the retinal pigment epithelium (RPE) layer in order to count the yellow points (pixels) indicating flow in each. Images were divided into three parts to reduce flow artifacts within the RPE layer: the choroid; a strip containing the RPE, interdigitation zone, and ellipsoid zone; and the retinal layers above the ellipsoid zone. To extract flow points (Fig. 2D-F), the RGB (red, green, blue) flow image was transformed into a gray-level image in which the intensity of each pixel was the average of the R and G values of the pixel in the RGB image, essentially generating the intensity of yellow in each pixel. These data were then used to analyze flow in the choroid and retinal regions (Fig. 2D) and to investigate the characteristics of the flow artifacts, as demonstrated in the strip region. For image analysis, the Otsu thresholding technique was used, which is based on black-and-white pixel segmentation in OCTA.[7] For an extended explanation, see the Appendix.

Statistical analysis

Analyses of covariance were used to assess observed differences between the preflight and postflight sessions. Mann-Whitney U test was used to compare the overall pixel count between time points and paired-samples Wilcoxon signed-rank test was used to address each slab between time points. All analyses were two-sided; significance was set at a p-value of 0.05. Statistical analyses were performed using Prism, version 7, and R, version 3.4.2 (R Development Core Team 2017).

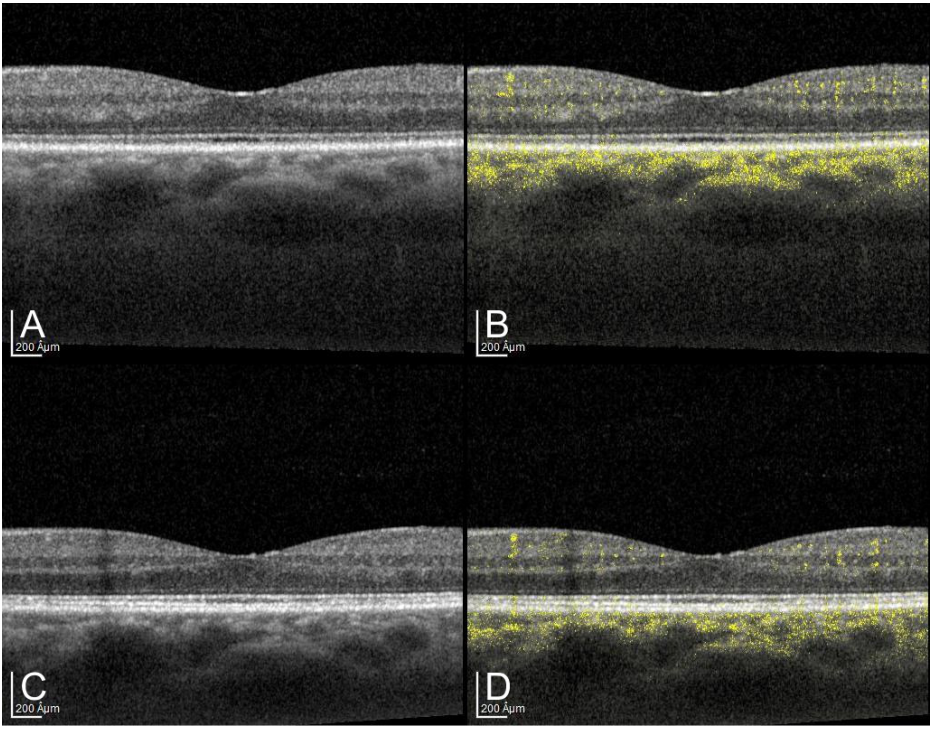

Fig. 1. Representative preprocessing image of postflight compared to preflight, dilatation of Haller's vessels in optical coherence tomography (OCT) and decrease in yellow dot density representing postflight flow as seen on cross-sectional B-scan ocular coherence tomography angiography (OCTA) images. *(A)* Preflight OCT. *(B)* Preflight OCTA with denser yellow dots compared to image 1D, representing more significant blood flow. *(C)* Postflight OCT. *(D)* Postflight OCTA. Note the lesser density of the dots compared to panel 1B, representing a less significant amount of blood. All images were made at the same anatomic location.

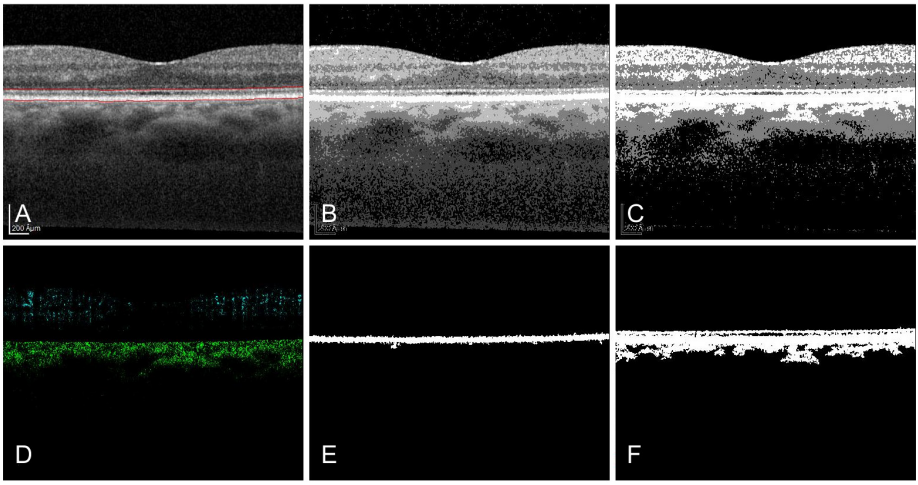

Fig. 2. Image processing and flow extraction of optical coherence tomography (OCT) and cross-sectional B-scan optical coherence tomography angiography (OCTA). *(A)* The lower boundary of retina and upper boundary of choroid (marked in red) on top of the original OCT image. The choroidal boundary is obtained using the image presented in panel D, and the retinal boundary is obtained using the image in panel F. *(B)* Five-level image (on five-level Otsu thresholding). *(C)* Three-level image (on three-level Otsu thresholding). *(D)* Choroidal flow (green) and retinal flow (light blue). *(E)* Binary image, obtained from panel B by keeping only the largest white object. (Other pixels in the image were changed to black.) *(F)* Binary image, obtained from panel C by keeping only the largest white object. (Other pixels in the image were changed to black.)

Results

The subject reported a severe headache on entering the International Space Station, which subsided slightly over the next 2 days but nevertheless persisted during his entire time in space. He also reported decompensation in near vision immediately upon entering space and a need for reading glasses (right eye: +2.25 sphere, left eye: +1.75 + 0.25 x 50) even though he did not use them in daily living.

Results of the preflight and postflight ocular examinations are shown in Table 1. The main differences on clinical examination were observed at the ocular surface: break-up time decreased from normal to < 2 seconds and corneas developed punctate epithelial erosion (PEE). Imaging demonstrated axial length shortening and no change in corneal tomography, which may account for the need of spectacles. The deterioration in the patient's near uncorrected vision may have been attributable to axial length shortening by 0.05 mm in the right eye and 0.08 mm in the left eye, which corresponded to the increase in choroidal vessel caliber shown on OCT (Fig. 3). There was a postflight mild decrease in central thickness in the retina

Table 1. Ocular examination before and after spaceflight

Variable	Preflight		Postflight	
	OD	OS	OD	OS
RAPD	Negative		Negative	
UCVA	20/25	20/20+2	20/20-2	20/20-1
Pinhole	20/20-1	NA	20/20+2	NC
Manifest refraction (BCVA)	+0.25 +0.50 *150 (20/20)	0 +0.50 *45 (20/15)	+0.25 +0.50 *150 (20/20+2)	-0.5 +1.75 *20 (20/20+2)
Ishihara	12/12	12/12	12/12	12/12
Pachymetry (mm)	560	556	567	565
Axial length (mm)	23.76	23.63	23.71	23.56
IOP*(mmHg)	9	9	11	12
Lid/lashes	Dermatochalsis +3		Dermatochalsis +3	
Schirmer (mm)	5	3	NA	NA
TBUT (seconds)	> 10	> 10	< 2	< 2
Cornea	Clear		PEE +2, Clear	
Conjunctiva	White/Quiet		White/Quiet	
Anterior chamber	Deep/Quiet		Deep/Quiet	
Lens	NS+1-2		NS+1-2	
Vitreous	Syneresis		Syneresis	
ONH C/D ratio	0.2		0.1	
Macula	Flat, normal reflex		Flat, normal reflex	
Vessels	Normal AV ratio		Normal AV ratio	
Peripheral	Attached, No RT/RD		Attached, No RT/RD	

AV: arteriovenous; BCVA: best-corrected visual acuity; IOP: intraocular pressure; mmHg: millimeter of mercury; NA: not applicable; NC: no change; NS: nuclear sclerosis; ONH C/D ratio: optic nerve head cup/disc ratio; OD: oculus dexter (right eye): OS: oculus sinister (left eye); PEE: punctate epithelial erosion; RAPD: relative afferent pupillary defect; RT/RD: retinal traction/retinal detachment; TBUT: tear breakup time; UCVA: uncorrected visual acuity
*Average of 3 measurements.

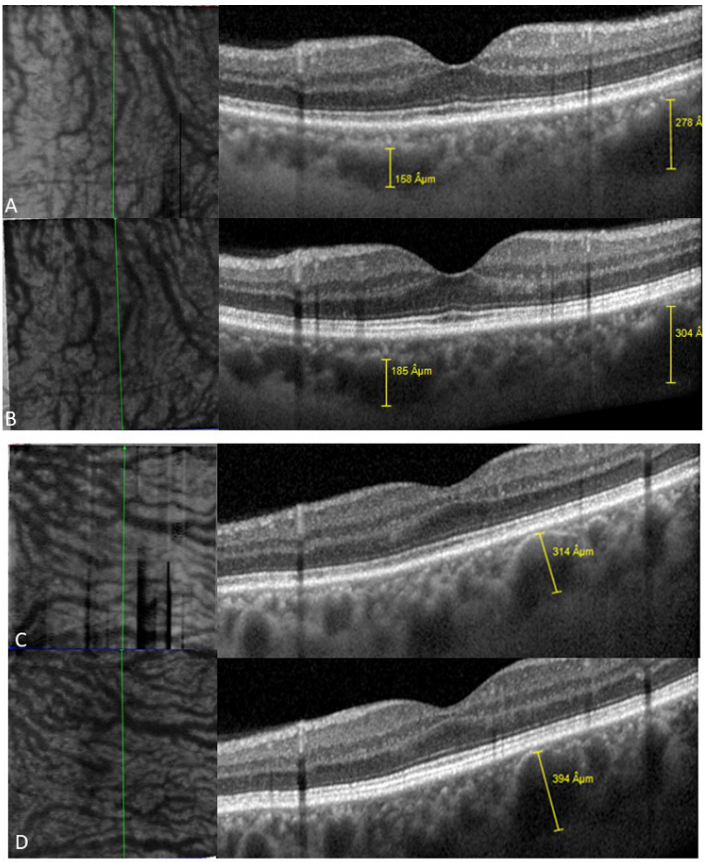

Fig. 3. Representation of the expansion in Haller's vessel caliber postflight compared to preflight using en-face and enhanced-depth optical coherence tomography (OCT) imaging. *(A, B)* Vertical tracked cross-sectional B-scan of the right eye indicating the location of Haller's vessels before and after flight, respectively. *(C, D)* Vertical tracked cross-sectional B-scan of the left eye indicating the location of Haller's vessels before and after flight, respectively. **The en-face panels represent the level of Haller's vessels.

and an increase in the central thickness of the choroid. Other clinical differences between the sessions were IOP increased insignificantly from 9 mmHg in both eyes to 11 mmHg in the right eye and 12 mmHg in the left. In the posterior segment, the preflight cup-to-disc ratio measured 0.2 in both eyes, and the postflight ratio was 0.1 in both eyes, even though no changes were seen on the OCT scans. No changes in distance vision or other parameters were noted. There was no notable change in visual fields on automated perimetry.

OCTA demonstrated a significant postflight decrease in the macular choroidal flow signal by 29% in the right eye and 11% in the left eye, and in the retinal flow signal by 8.5% and 6.5%, respectively ($p < 0.0001$ for both factors for both eyes; Fig. 3). The greatest morphological effect was observed in the choroid (Table 2), where the decrease in the flow signal was accompanied by focal dilatations of the mid/large choroidal vessels (Fig. 4). No significant alterations were found in other structural parameters compared to baseline. Mild optic nerve sheath widening was noted bilaterally on MRI (Fig. 5). Preflight optic nerve sheaths were 5.80 mm in the right eye and 6.15 mm in the left eye; postflight values, measured at the same distance from the optic nerve by an experienced neuroradiologist, were 6.92 mm and 6.90 mm, respectively. Diffusion-weighted imaging revealed bilateral accumulation of fluid around the optic nerves.

Table 2. Structural ocular characteristics, preflight and postflight sessions, obtained by OCT

Variable	Eye	Preflight	Postflight
Optic nerve head analysis			
Retinal nerve fiber layer thickness (µm)	OD	96	97
	OS	94	97
Bruch's membrane opening area (mm^2)	OD	1.74	1.81
	OS	1.63	1.64
Minimum rim width (µm)	OD	382	384
	OS	388	416
Optic nerve sheath (mm)	OD	5.8	6.92
	OS	6.15	6.90
Peripapillary wrinkles	OU	none	none
Retina and choroid analysis			
Central macular thickness (µm)	OD	285	282
	OS	289	280
Central choroidal thickness (µm)	OD	270	301
	OS	405	431
Choroidal/retinal folds	OU	none	none

OD: oculus dexter (right eye); OS: oculus sinister (left eye); OU: oculus uterque (both eyes)

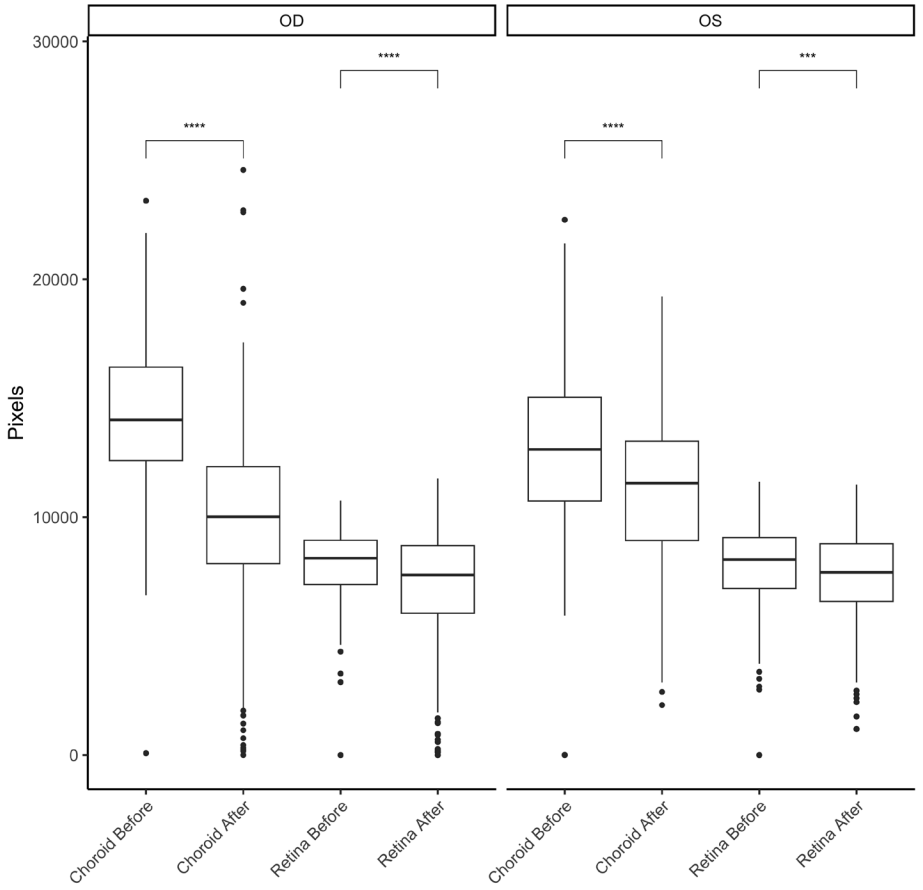

Fig. 4. Comparison of choroidal and retinal optical coherence tomography angiography (OCTA) flow signal quantification for each eye between preflight and postflight conditions. The Y axis represents the total amount of signal measured by pixels for each slab. ****p* < 0.001, ***** p* < 0.0001

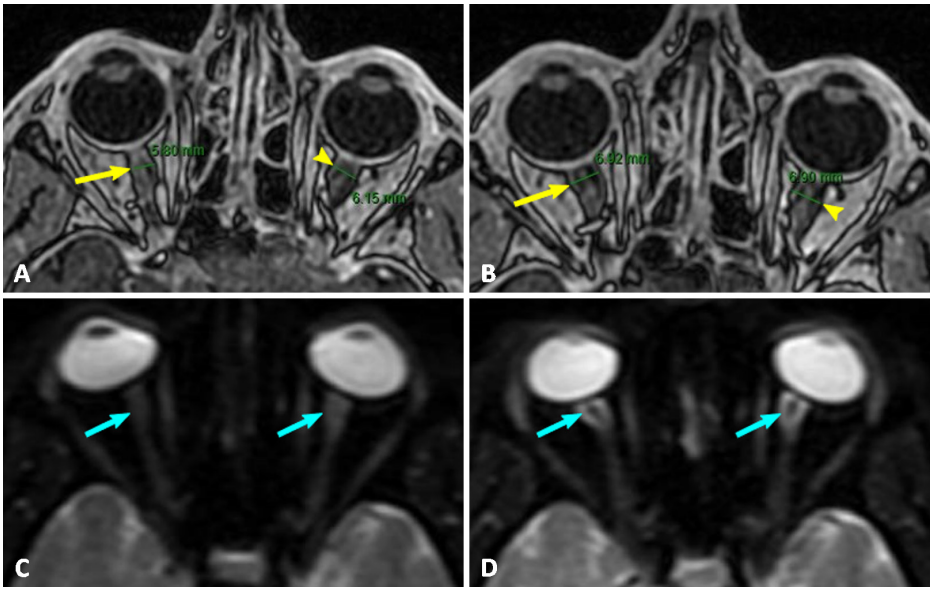

Fig. 5. Magnetic resonance imaging (MRI) scans of the astronaut orbits: T1-weighted MRI *(A)* preflight, *(B)* postflight. Images were taken less than 24 hours after return of the astronaut to Earth. Note the widening of the optic nerve sheath in mm. Diffuse weighted MRI scans, *(C)* preflight, *(D)* postflight. Note the excessive postflight fluid around the optic nerve compared to the preflight state. Arrow points to right optic nerve. Arrowhead points to the left optic nerve.

Discussion

The main finding of this investigation was a postflight decrease in OCTA flow signal in the choroidal vessels in the context of choroidal vessel dilation, which could be indicative of relative venous congestion. Among the wide spectrum of ophthalmic imaging parameters evaluated (Tables 1 and 2), the most prominent alterations were demonstrated on structural and angiographic analysis of the retinal and choroidal vasculature. OCT revealed focal dilatation of Haller's vessels, and OCTA revealed a decrease in retinal and choroidal flow. Based on the work of Federico *et al.*, the percentage of change in OCTA signal strength ranges from 0% to 9.8%.[8] This report expands our understanding of the ocular alterations that may occur after a short-duration spaceflight and may provide insight into the underlying mechanism of SANS. As such, OCTA may serve as a promising addition to the standard protocol for evaluation of the eye in astronauts.

The microgravity environment associated with spaceflight causes a cephalic shift in blood and cerebrospinal fluid that results in a constellation of unique ocular clinical

and imaging findings.[1] It has been suggested that venous congestion in the head and orbit leads to elevated vortex venous pressure and reduced choroidal drainage, with consequent pooling of blood in the choroid.[3] SANS has been associated with choroidal thickening and the development of cilioretinal folds.[3] We observed some degree of choroidal thickening, with no chorioretinal folds. These findings may represent early structural adaptations to microgravity exposure. Based on prior long-duration mission data, choroidal thickening appears to correlate with mission duration and may only partially regress postflight; however, the short exposure in the present case precludes conclusions regarding progression or permanence.[2-4] Mader *et al.* found the choroidal thickening to be less pronounced upon return of astronauts to Earth, but it did not revert to baseline thereafter.[2] They hypothesized that the choroidal pooling causes gradual modification of the collagen lamella beyond the normal anatomic boundaries, leading to permanent distention even after the restoration of normal venous flow. Previous OCTA studies that characterized the vascular networks of the retina and choroid in healthy individuals stressed the wide variability among the different OCTA devices from different manufacturers, showing that the data could not be used interchangeably.[8,9] Nevertheless, repeatability was high when the same scanning protocol was used with the same OCTA device on different occasions.[8]

Choroidal circulation is complicated and multifactorial, and OCTA devices have only limited ability to demonstrate flow in the deeper Sattler's and Haller's layers of the choroid because the flow velocity is low relative to the motion threshold. In the present study, to minimize data loss due to segmentation and projection artifacts of the device during analysis of the retinal and choroidal flow signal, image processing analysis of 512 scans with flow overlay (Fig. 2A-F; Appendix) was performed before and after spaceflight. The results demonstrated a significant decrease in choroidal and retinal flow upon return of the astronaut to Earth.

It has been shown that the choroidal circulation is dependent on the ocular perfusion pressure.[10] Thus, systemic conditions such as microgravity that affect changes in ocular perfusion may result in changes in choroidal perfusion. Aqueous humor production and outflow are primarily driven by active metabolic secretion and pressure gradients, as seen in the Goldmann equation, which are not inherently gravity-dependent.[11] In addition, IOP changes observed during spaceflight are generally mild, suggesting that alterations in the TLPD are primarily driven by changes in ICP rather than IOP.[2] Because IOP measurements were obtained pre- and postflight, transient inflight fluctuations cannot be excluded. Changes in choroidal blood flow have also been associated with postural changes. Longo *et al.* found that mean choroidal blood flow assessed by laser Doppler flowmetry increased significantly when the body was tilted from the upright to the supine position.[12] In the present study, the findings on OCTA were supported by the bilateral change in the optic nerve sheath on T1-weighted MRI (Fig. 5A,B) and by the excessive fluid surrounding the optic nerve on diffusion-weighted MRI (Fig. 5C,D). No signs of elevated ICP and

no breaks in the blood-retina barrier were noted using OCTA. Despite changes in corneal tear breakup time, imaging modalities including corneal tomography and ultrasound, biometry, and visual field tests did not reveal meaningful anatomical or functional changes.

The strength of this study is the early and wide variety of clinical and imaging examinations conducted upon return of the astronaut to Earth. All assessments were performed by a single operator using identical imaging protocols with the same imaging devices both pre- and postflight. The main limitations of the study are the single-case evaluation and short duration of the spaceflight. In addition, the imaging sessions were not performed in space.

Conclusion and future perspectives

In conclusion, the etiology of SANS is still unknown. This case report of a single astronaut highlighted the bilateral axial length shortening and choroidal vessel thickening related to spaceflight. From a systemic perspective, the common pathway of blood drainage from the eye-brain axis to the internal carotid artery passes through the cavernous sinus, which drains the ophthalmic, cerebral, middle meningeal, and pterygoid veins. Venous congestion in this common pathway could account for the cephalad fluid shift reported in microgravity environments which, in turn, might lead to choroidal venous congestion and, later, to SANS-related ocular manifestations. In our subject, the venous congestion could have caused an increase in choroidal thickness and structural dilatation of Haller's vessels, consequently exacerbating the decrease in the choroidal flow signal, demonstrated for the first time using OCTA. Thus, the use of OCTA in this setting may broaden our knowledge and understanding of the changes in choroidal-retinal blood flow after spaceflight and their link to SANS.

Declarations

Ethics approval and consent to participate

The study was conducted in accordance with the Declaration of Helsinki, and the study protocol was approved by the Institutional Review Boards of Rabin Medical Center, Petach Tikva, Israel and the University of Central Florida, Orlando, Florida, USA. Consent to publish this report was obtained from the subject in writing.

Competing interests

Professor Alon Harris received remuneration from AdOM, Qlaris, and Cipla for serving as a consultant and is a member of the board of AdOM, Qlaris and SlitLed. Professor Alon Harris holds ownership interest in AdOM, Oxymap, Qlaris, and SlitLed. Professor Alon Harris serves as Chief Editor of AIVO; at no point before manuscript acceptance was he involved in the publication process. AIVO conducts single-blind peer review.

Funding
This work was supported by the Department of Ophthalmology, Rabin Medical Center. Professor Alon Harris is supported by US National Institutes of Health grants (R01EY030851 and R01EY034718), NYEE Foundation grants, The Glaucoma Foundation grant, and in part by a Challenge Grant award from Research to Prevent Blindness, NY.

Acknowledgments
We thank Dr. Harel Baris for his support in executing the protocol. MRI data were obtained from the research group at Sheba Medical Center, led by Dr. Itzik Cooper and Professor Yael Mardor, as part of the ARC Space Lab activities. We thank Dr. Vadim Hadminski, from Hasharon Medical Center, for analyzing the MRI, and the team from Heidelberg Engineering—Rami Libenthal, Steve Thomas and Karen McHugh—for their great efforts and support of this project.

References

1. Nelson ES, L. Mulugeta L, Myers JG. Microgravity-induced fluid shift and ophthalmic changes, Life (Basel). 2014;4:621-65. https://doi.org/10.3390/life4040621
2. Mader TH, Gibson CR, Pass AF, et al. Optic disc edema, globe flattening, choroidal folds, and hyperopic shifts observed in astronauts after long-duration space flight. Ophthalmology. 2011;118:2058-2069. https://doi.org/10.1016/j.ophtha.2011.06.021
3. Lee AG, Mader TH, Gibson CR, et al. Spaceflight associated neuro-ocular syndrome (SANS) and the neuro-ophthalmologic effects of microgravity: A review and an update. NPJ Microgravity. 6 2020;6:7. https://doi.org/10.1038/s41526-020-0097-9
4. Ong J, Tarver W, Brunstetter T, et al. Spaceflight associated neuro-ocular syndrome: Proposed pathogenesis, terrestrial analogues, and emerging countermeasures, Br J Ophthalmol. 2023;107:895-900. https://doi.org/10.1136/bjo-2022-322892
5. Stern C, Yücel YH, Zu Eulenburg P, Pavy-Le Traon A, Petersen LG. Eye-brain axis in microgravity and its implications for Spaceflight Associated Neuro-ocular Syndrome. NPJ Microgravity. 2023;20:56. https://doi.org/10.1038/s41526-023-00300-4
6. de Carlo TE, Romano A, Waheed NK, Duker JS. A review of optical coherence tomography angiography (OCTA), Int J Retina Vitreous. 2015;1:5. https://doi.org/10.1186/s40942-015-0005-8
7. Meiburger KM, Salvi M, Rotunno G, Drexler W, Liu M, Automatic segmentation and classification methods using optical coherence tomography angiography

(OCTA): A review and handbook. Appl Sci. 2021;11:9732. https://doi.org/10.3390/app11209734

8. Corvi F, Corradetti G, Parrulli S, Pace L, Staurenghi G, Sadda SR. Comparison and repeatability of high resolution and high speed scans from spectralis optical coherence tomography angiography. Transl Vis Sci Technol. 2020;9:29. https://doi.org/10.1167/tvst.9.10.29
9. Lei J, Pei C, Wen C, Abdelfattah NS. Repeatability and reproducibility of quantification of superficial peri-papillary capillaries by four different optical coherence tomography angiography devices. Sci Rep. 2018;8::17866. https://doi.org/10.1038/s41598-018-36279-2
10. Schmidl D, Garhofer G, Schmetterer L. The complex interaction between ocular perfusion pressure and ocular blood flow - relevance for glaucoma. Exp Eye Res 2011;93:141-155. https://doi.org/10.1016/j.exer.2010.09.002
11. Huang AS, Stenger MB, Macias BR. Gravitational Influence on Intraocular Pressure: Implications for Spaceflight and Disease. J Glaucoma. 2019 Aug;28(8):756-764. https://doi.org/10.1097/IJG.0000000000001293
12. Longo A, Geiser MH, Riva CE, Posture changes and subfoveal choroidal blood flow. Invest Ophthalmol Vis Sci. 2004;45:546-551. https://doi.org/10.1167/iovs.03-0757

Appendix: Image-processing algorithm

Image extraction

The input to the image-processing algorithm consisted of two sets of 512 JPEG images obtained from the optical coherence tomography (OCT) scanner (OCT2, Heidelberg, Germany), displaying 512 retinal slices before and after the flight.

Each image contained a joint display of the structural OCT image, an image showing the optical coherence tomography angiography (OCTA) flow data, represented by yellow points (pixels), overlaying the structural OCT image, and an image showing the OCTA flow without structural information. Each sub-image was extracted separately from the joint image. Omitting the top 96 rows (dark background above the retina) yielded structural and flow images for each slice measuring 400 x 512 pixels. The size was actually 400 x 512 x 3 because the images were in red-green-blue (RGB) format.

Image processing

Step 1: Separation to regions

The aim of image processing was to identify and count the points (pixels) indicating flow in each slice, while separating the flow in the retinal region (*i.e.*, the layers containing the retinal network) from the flow in the choroid. Thus, in each structural image, the algorithm identified the lower boundary of the retinal pigment epithelium (RPE) and the upper boundary of the ellipsoid zone, thereby dividing the image into three parts: the choroid; a strip containing the RPE, interdigitation zone, and ellipsoid zone; and the retinal layers above the ellipsoid zone (see Fig. 2A). Since the strip (which appears bright in the image) does not contain real blood flow (but includes artifacts), separating it from the region above enabled flow analysis in the latter region with fewer artifacts.

To identify the lower boundary of the RPE, we applied image segmentation to the structural image using five-level Otsu thresholding.[1,2] The resulting five-level image (see Fig. 2B) was transformed into a binary image by merging the four lower gray levels. The largest bright object in the resulting image (which contained the RPE) was then identified. If the length of the object was less than 90% of the width of the image (meaning that parts of the RPE were missed and appear as separate objects), morphological closing and opening[3] were applied to the binary image to eliminate gaps in the RPE and clean noise. The largest object was then extracted again, and all other bright pixels were erased (see Fig. 2E). The lower boundary

of the RPE was extracted by identifying the lowest bright pixel in each column of image and erasing the rest. If the boundary curve did not reach the left or the right edge of the image, the missed part was filled with a straight horizontal line from the leftmost/rightmost boundary pixel identified to the edge of the image.

The method for initial identification of the upper boundary of the ellipsoid zone was similar to that described above (see Fig. 2C,F). Instead of using five-level Otsu thresholding, we used three-level Otsu thresholding (see Fig. 2C), merging the two lower levels, and applying slightly different morphological operations (closing and opening) with different structuring elements. Since the curve obtained from the upper bright pixel in each image column was inaccurate in many cases, we used it only as an initial upper boundary of the strip. We then computed, in each column, the vertical difference between this upper boundary and the previously obtained lower boundary of the RPE and calculated the average value. This value plus 1 was defined as the desired width of the bright strip.

Finally, we used the lower boundary of the RPE as the lower boundary of the strip, and an identical curve whose distance from the lower boundary was the above-defined strip width was used as the upper boundary of the strip.

Step 2: Extraction of flow points

The next step of the algorithm was to identify the yellow points (pixels) representing flow in the flow images. The RGB flow image was transformed into a gray-level image in which the intensity of each pixel was the average between the R and G values of the pixel in the RGB image. This value represented the intensity of yellow in each pixel.

Hypothetically, each pixel with an intensity greater than zero indicates blood flow. However, in practice, the background contained many pixels with greater intensities. Any yellow flow signal present in structures known to be avascular is a projection artifact. Highly reflective structures, such as the external limiting membrane, ellipsoid zone, and RPE/photoreceptor interdigitation zone, generally exhibit more projection artifacts, and a flow signal will often be recorded. It is important to remember that the yellow points representing flow simply indicate regions where the OCTA algorithm has recorded a change between successive B-scans and assigned this signal as flow. No velocity information can be derived from this display. To avoid identifying the background as flow, we empirically chose a threshold value for flow after consulting with Heidelberg's engineers. All pixels whose intensity was less than or equal to 10 were nulled, thereby eliminating most of the background points. Since we had previously found the boundaries of the bright strip, we were able at that stage to count the number of flow points in each region (choroid, strip, retinal) separately. This was done for every slice, in both image sets (pre- and postflight). The data thus obtained were then used to analyze the flow in the choroid and retinal regions as well as to investigate the characteristics of the flow artifacts as demonstrated in the strip region.

References

1. Otsu N. A threshold selection method from gray level histograms. IEEE Trans Sys Man Cyber. 1979;9:62–66.
2. Liao PS, Chen TS, Chung PC. A fast algorithm for multilevel thresholding. J Inf. Sci. Eng. 2001;17:713–727.
3. Gonzalez RC, Woods RE. Digital Image Processing, 4th edition. Pearson; New York: 2018, pp. 702-705.